Simultaneous structure and elastic wave velocity measurement of SiO2 glass at high pressures and high temperatures in a Paris-Edinburgh cell

Yoshio Kono, Changyong Park, Tatsuya Sakamaki, Curtis Kenny-Benson, Guoyin Shen et al.

Related Articles

Analysis of the particle stability in a new designed ultrasonic levitation device
Rev. Sci. Instrum. 82, 105111 (2011)

Modeling of ultrasound transmission through a solid-liquid interface comprising a network of gas pockets
J. Appl. Phys. 110, 044910 (2011)

Combined ultrasonic elastic wave velocity and microtomography measurements at high pressures
Rev. Sci. Instrum. 82, 023906 (2011)

A broadband spectroscopy method for ultrasonic wave velocity measurement under high pressure
Rev. Sci. Instrum. 82, 014501 (2011)

Picosecond ultrasonic experiments with water and its application to the measurement of nanostructures
J. Appl. Phys. 107, 103537 (2010)

Additional information on Rev. Sci. Instrum.

Journal Homepage: http://rsi.aip.org

Journal Information: http://rsi.aip.org/about/about_the_journal

Top downloads: http://rsi.aip.org/features/most_downloaded

Information for Authors: http://rsi.aip.org/authors
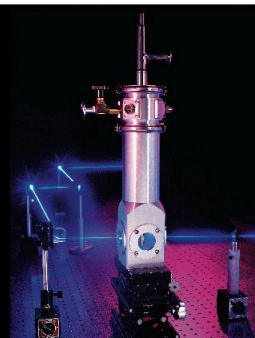
Simultaneous structure and elastic wave velocity measurement of SiO₂ glass at high pressures and high temperatures in a Paris-Edinburgh cell

Yoshio Kono,[1] Changyong Park,[1] Tatsuya Sakamaki,[2] Curtis Kenny-Benson,[1] Guoyin Shen,[1] and Yanbin Wang[2]

[1]*High Pressure Collaborative Access Team (HPCAT), Geophysical Laboratory, Carnegie Institution of Washington, 9700 S. Cass Ave., Argonne, Illinois 60439, USA*
[2]*GeoSoilEnviroCARS, Center for Advanced Radiation Sources, The University of Chicago, 5640 S. Ellis Avenue, Chicago, Illinois 60637, USA*

An integration of multi-angle energy-dispersive x-ray diffraction and ultrasonic elastic wave velocity measurements in a Paris-Edinburgh cell enabled us to simultaneously investigate the structures and elastic wave velocities of amorphous materials at high pressure and high temperature conditions. We report the first simultaneous structure and elastic wave velocity measurement for SiO₂ glass at pressures up to 6.8 GPa at around 500°C. The first sharp diffraction peak (FSDP) in the structure factor S(Q) evidently shifted to higher Q with increasing pressure, reflecting the shrinking of intermediate-range order, while the Si-O bond distance was almost unchanged up to 6.8 GPa. In correlation with the shift of FSDP position, compressional wave velocity (Vp) and Poisson's ratio increased markedly with increasing pressure. In contrast, shear wave velocity (Vs) changed only at pressures below 4 GPa, and then remained unchanged at ∼4.0–6.8 GPa. These observations indicate a strong correlation between the intermediate range order variations and Vp or Poisson's ratio, but a complicated behavior for Vs. The result demonstrates a new capability of simultaneous measurement of structures and elastic wave velocities at high pressure and high temperature conditions to provide direct link between microscopic structure and macroscopic elastic properties of amorphous materials. © *2012 American Institute of Physics.* [http://dx.doi.org/10.1063/1.3698000]

I. INTRODUCTION

Correlation between structure and physical properties is fundamental for understanding the behavior of materials. For crystalline materials, both structure and physical properties have been widely studied at high pressure and high temperature conditions by integrating high-pressure apparatus (e.g., large volume press, diamond anvil cell) with various measurement techniques. In contrast, those of liquids and amorphous solids have been much less studied due to experimental difficulties. Some efforts have been made to investigate structure of amorphous materials (e.g., Refs. [1–4]), physical properties such as density (e.g., Refs. [5–8]), viscosity (e.g., Refs. [7] and [9]), and elastic wave velocities (e.g., Refs. [10] and [11]). However, these results were often based on individual techniques, and the discussions were made by comparisons with results from other techniques. Integrating these techniques should promote a more comprehensive understanding of the behavior of amorphous materials. In this paper, we report a new experimental capability allowing for simultaneous measurements of amorphous structures and elastic wave velocities at high pressure and high temperature conditions.

Elastic wave velocity has been considered to be highly sensitive to structural changes. The measurements of elastic wave velocities of several amorphous materials have implied associated structural changes (e.g., Refs. [12] and [13]). In addition, some researchers have used elastic wave velocities to understand compression behavior of amorphous materials at high pressures by deriving the bulk modulus-density relationship from compressional (Vp) and shear (Vs) wave velocities

as follows:

$$\rho_P = \rho_0 + \int_{P_0}^{P} \frac{1 + \alpha \gamma T}{\left(Vp^2 - 4/3Vs^2\right)} dP,$$

where ρ_P and ρ_0 are densities at pressure P and ambient pressure P_0, respectively (e.g., Refs. [10] and [14]). The coefficient $1 + \alpha \lambda\, T$ is the conversion ratio of adiabatic to isothermal bulk modulus, where α, λ, and T is thermal expansion coefficient, Grüneisen parameter, and temperature in Kelvin. When the compression of amorphous material is elastic under hydrostatic pressure without any structural transformations or irreversible densifications, use of this equation allows us to obtain the pressure-density equations of state from Vp and Vs measurements. Furthermore, elastic wave velocities of candidate materials, in conjunction with seismological observations of the Earth's interior, provide one of the most important parameters to model the nature of the inaccessible Earth's interior. Thus, elastic wave velocity is important not only to understand physics of the amorphous materials but also to be useful for Earth science.

Sector 16-BM-B, HPCAT at the Advanced Photon Source (APS), is capable of conducting structure measurement of liquid and glass at high-pressure and high-temperature conditions in a Paris-Edinburgh cell by using multi-angle energy-dispersive x-ray diffraction (Ref. [4]). In addition to the structure measuring capability, we have newly developed a setup of ultrasonic and x-ray radiography measurement at the beamline in order to determine elastic wave travel time and sample length, respectively, and the resultant

elastic wave velocities. Here we report the first simultaneous structure and elastic wave velocity measurement at high pressure and high temperature conditions for SiO_2 glass for demonstration of the new experimental capability.

II. EXPERIMENTAL METHODS

Figure 1(a) shows the schematic illustrations of the experimental setup with a Paris-Edinburgh press at the 16-BM-B white x-ray station, the APS. The incident white x-rays were collimated by two pairs of slits made of tungsten, and diffracted x-rays were collimated horizontally by a fixed gap (50 μm) slit in the closest vicinity of the sample and slits in front of a Ge solid state detector (Ge-SSD). A large Huber stage holding the Ge-SSD allows us to precisely control 2θ angle. The energy of the Ge-SSD was calibrated by using NIST radioactive sources (Co^{57} and Cd^{109}) and the 2θ angles were calibrated by using unit-cell parameter of MgO at ambient condition.

High-pressure experiment was carried out using a Paris-Edinburgh (PE) press (e.g., Ref. 15). We used cupped anvils with 3 mm diameter flattened bottom (cf. Ref. 4). We combined the cell assembly designs from those previously reported for high-pressure melt structure measurement (Ref. 4) and for high pressure and room temperature ultrasonic measurement (Ref. 11) in order to conduct the both structure and ultrasonic measurements at high pressure and high temperature conditions. The modified cell assembly mainly consists of zirconia (ZrO_2) caps and a boron epoxy gasket, which provide good thermal insulation for high-temperature experiments (Fig. 1(b)). Heating was conducted using a graphite sleeve heater. Temperature was measured by a WRe5%-WRe26% thermocouple. An alumina (Al_2O_3) buffer rod was placed between tungsten carbide (WC) anvils and the sample to adjust the position of sample for taking x-ray radiography image around the sample, which enables us to determine sample length at high pressure and high temperature conditions. The sample was silica (SiO_2) glass with a thickness of 0.430 mm and a diameter of around 2.5 mm in cylindrical shape. Both ends of the sample and the Al_2O_3 buffer rod were polished with 1 μm diamond paste to maximize mechanical contact for elastic wave propagation. In order to further increase the mechanical contact between the Al_2O_3 buffer rod and the sample and to provide a mark of the interface, 2.5 μm Au foil was inserted between the buffer rod and the sample. In contrast, copper (Cu) was used as a backing reflector, which causes strong ultrasonic reflection at the interface. Pressure was determined by the equation of state of Al_2O_3 (Ref. 16). The unit-cell volume of Al_2O_3 was measured by energy-dispersive x-ray diffraction at a 2θ angle of $10°$.

The *in situ* structure measurements were carried out by the multi-angle energy-dispersive x-ray diffraction (EDXD) (Ref. 4). In this study, the EDXD patterns were collected at $3°$, $4°$, $5°$, $7°$, $10°$, $14°$, $20°$, and $25°$. To keep the dead time of the Ge-SSD to be less than 15%, the size of the slits was adjusted for each 2θ angle. In addition, acquisition time was adjusted to achieve an intensity of around 2500 counts at the maximum for each 2θ angle. As a result, the measurement took around 2–3 h depending on the details of optimized counting
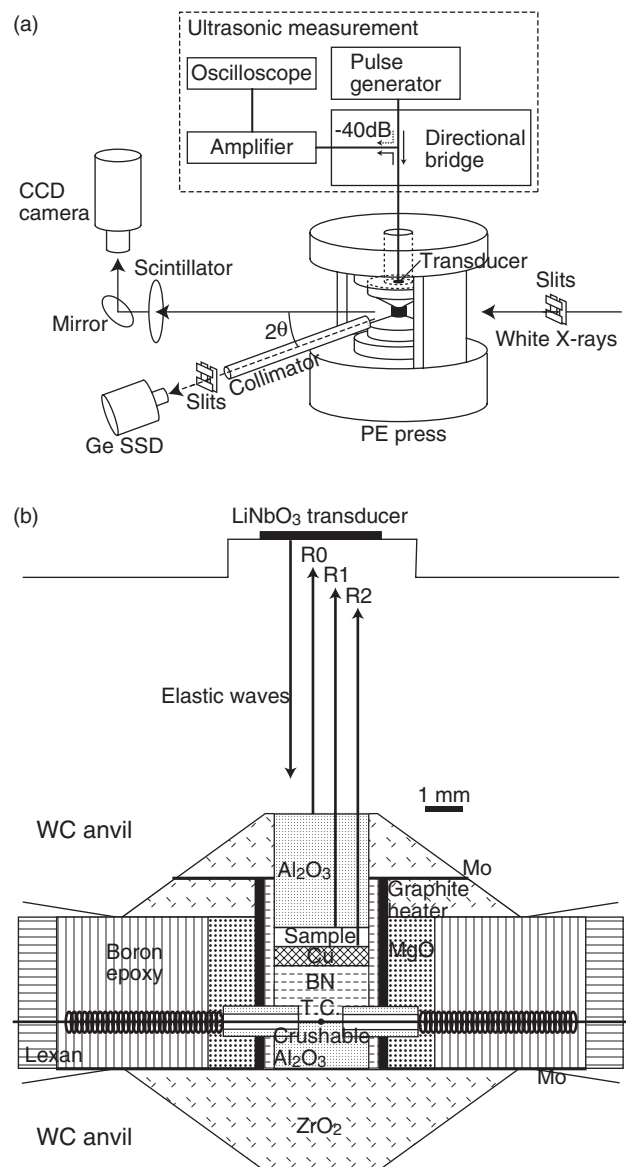

FIG. 1. (a) Schematic illustrations of the experimental setup for the combined multi-angle energy-dispersive x-ray diffraction, ultrasonic, and x-ray radiography measurements in a Paris-Edinburgh (PE) press. (b) Illustration of the high-pressure and high-temperature experimental cell assembly and WC anvil. The LiNbO$_3$ transducer attached behind the top WC anvil generates and receives elastic waves. Elastic waves path through the WC anvil and propagate into Al_2O_3 buffer rod and the SiO_2 glass sample.

conditions at each angle. Analysis of the obtained multi-angle energy dispersive x-ray diffraction data was conducted using a software package by K. Funakoshi described in Ref. 17.

The elastic wave velocity measurements were conducted also *in situ* on exactly the same sample and the conditions. Similarly to the previous studies (e.g., Refs. 11 and 18), we attached the ultrasonic transducer to opposite ends of the top WC anvil and the co-axial cable was connected through a hole at the top of the PE press (Fig. 1). A $10°$ Y-cut LiNbO$_3$ transducer was used to generate and receive both compressional and shear waves simultaneously (e.g., Ref. 19). Electrical sine waves of 20 MHz (for shear wave) and 30 MHz (for compressional wave) with an amplitude of 1.5 $V_{peak-to-peak}$ were generated by a pulse generator (Tektronix AFG3251). The

electrical signals were divided into two directions by a directional bridge (Agilent RF Bridge 86205A). One signal was directed to an oscilloscope through a -40 dB attenuation path and the other signal went to the $LiNbO_3$ transducer through the directional bridge. Elastic waves generated by the $LiNbO_3$ transducer passed through the WC anvil and propagated into the Al_2O_3 buffer rod and the sample. A series of reflected elastic wave signals came from the interfaces of anvil/buffer rod (R0), buffer rod/sample (R1), and sample/backing reflector (R2). These series of reflected signals and the attenuated input signal were amplified by a 40 dB amplifier with a bandwidth of 0.2–40 MHz (Olympus Model 5678 Ultrasonic Preamplifier). Then the signals were acquired with a sampling rate of 10×10^9 sample/s (0.1 ns interval at each sampling) by a digital oscilloscope (Tektronix DPO5104).

Figure 2(a) shows an example of waveform obtained for the SiO_2 glass sample. The data show clear reflected signals of R0, R1, and R2 for both compressional and shear wave. The elastic wave travel time was determined by the pulse echo overlap method using the reflected signals from the buffer rod/sample (R1) and sample/backing reflector (R2) interfaces (Fig. 2(b)). Since the acoustic impedance of the Cu backing reflector is larger than that of the SiO_2 glass sample, the sample/backing reflector (R2) interfaces yielded a negative reflection coefficient ($= (Z_S - Z_{Cu})/(Z_S + Z_{Cu})$, Z_S and Z_{Cu} are acoustic impedances of the sample and the Cu backing reflector, respectively). Therefore, the R2 signal was inverted to be overlapped with the R1 signal. In the travel time analysis, we first roughly selected a reference peak position in phase for the R1 and R2 signals, respectively. Then the R2 signal was overlapped with the R1 signal for the scanning time window of ± 5 ns with the interval of 0.1 ns ($=$ sampling rate of oscilloscope), and we took cross correlation between R1 and R2 signals at each step. Figure 2(c) shows a result of the travel time analysis for the wave shown in Fig. 2(b). Cross correlation parameter changed with varying overlap time, and the peak position corresponds to two-way travel time of the elastic wave through the sample. The peak position was well defined within the uncertainty of ± 1 step (± 0.1 ns). The uncertainty of ± 0.1 ns in the travel time analysis yielded the resultant uncertainty in compressional and shear wave velocities of up to $\pm 0.08\%$ and $\pm 0.05\%$, respectively.

The travel distance of the elastic waves, corresponding to the sample length, was determined by x-ray radiography, which is critical to accurately determine the elastic wave velocities based on the measured travel time above. We used Tb-doped gadolinium gallium garnet (GGG:Tb) thin film single crystal (5 μm) deposited on undoped GGG as a scintillator, and the transmission image was acquired by an interline CCD camera (Prosilica GC1380) with 1360 (horizontal) $\times$ 1024 (vertical) pixels. The pixel resolution was calibrated by using the initial sample length of the SiO_2 glass at ambient pressure (430 μm), which was measured by a micrometer before the experiment. The calibration yielded 0.948 μm/pixel resolution, which correspond to around 1.3 (horizontal) $\times$ 1.0 (vertical) mm full field of view or $6.8\times$ magnification based on the known unit cell size (6.45 μm) of the CCD camera.

Figure 3(a) shows an example of the observed x-ray radiography image around the SiO_2 glass sample. The boundary between the Al_2O_3 buffer rod and the SiO_2 glass sample
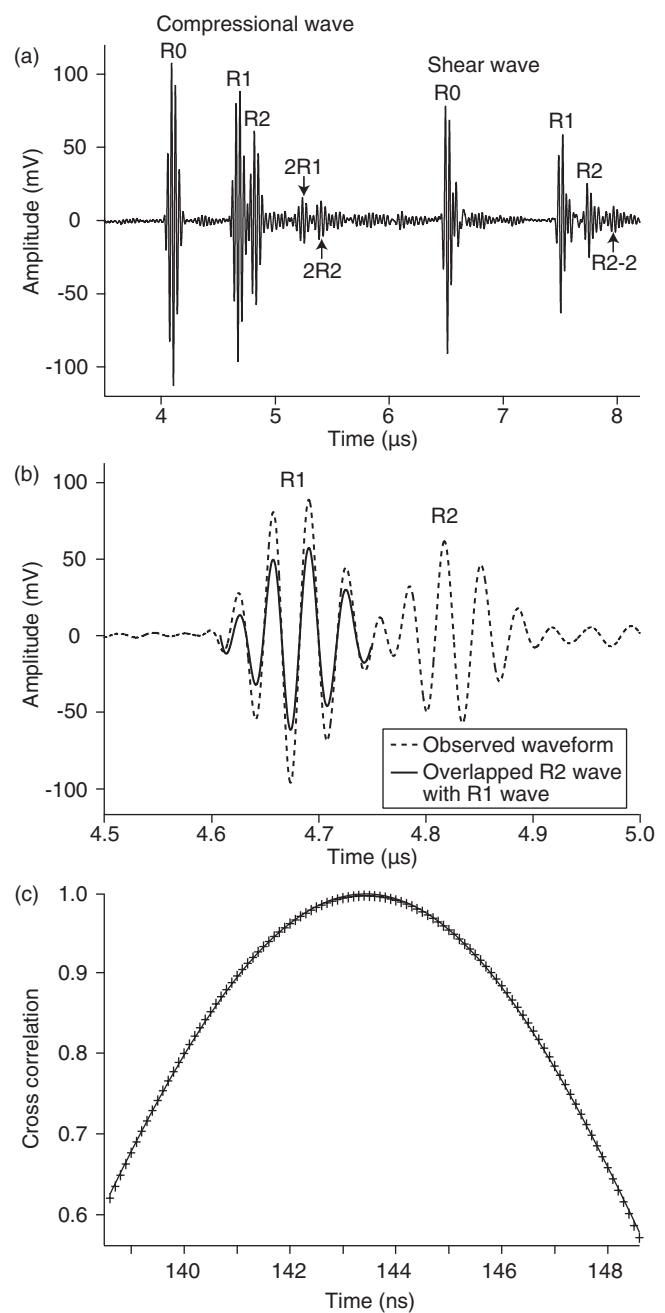

FIG. 2. (a) An example of compressional and shear wave signals reflected at anvil/buffer rod (R0), buffer rod/sample (R1), and sample/Cu (R2) interfaces at pressure of 1.2 GPa. The 2R1 and 2R2 is the second buffer rod/sample reflection and the corresponding reflection at the sample/Cu interface, respectively. The R2-2 is the twice two-way traveled signal from the sample. (b) Enlarged view of the R1 and R2 signals of compressional wave. Elastic wave travel time was determined by pulse echo overlap method. Since reflection coefficient at the sample/Cu (R2) interface is negative, the R2 signal was overlapped with R1 signal after inverting the R2 signal. (c) A result of cross correlation curve as a function of overlap time analyzed for the R1 and R2 signals in Fig. 2(b). The cross symbols represent results of each step, and the line is the result of curve fit to determine peak position, which corresponds to two-way travel time of elastic wave.

ary between the Al_2O_3 buffer rod and the SiO_2 glass sample was marked by a strong absorption due to the 2.5 μm Au foil. On the other hand, another boundary between the SiO_2 glass sample and the Cu backing reflector was found by strong brightness change between SiO_2 and Cu. The position of the buffer rod/sample interface was determined by the peak
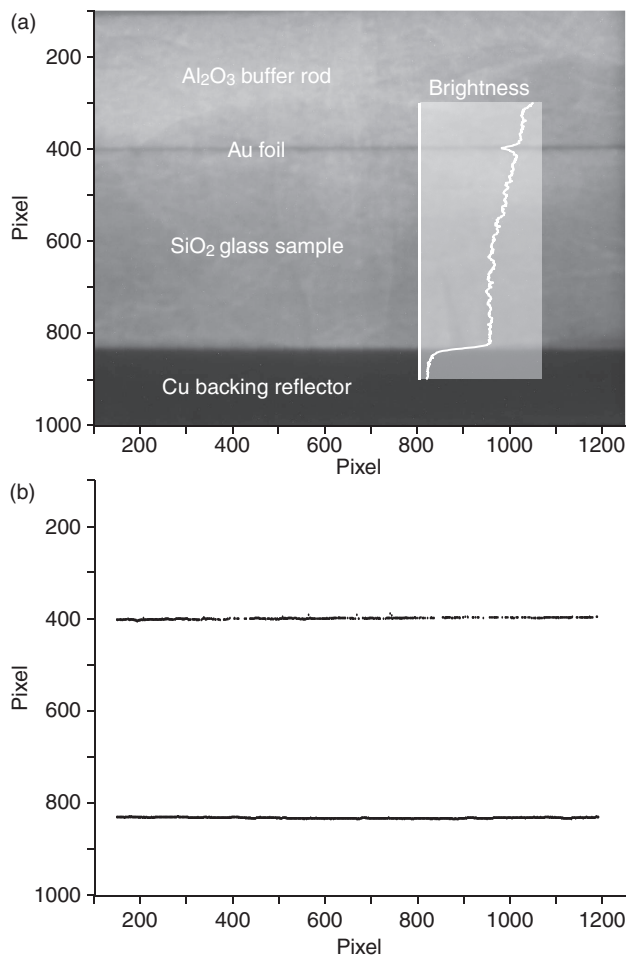
FIG. 3. (a) An example of x-ray radiography image around the sample at pressure of 1.2 GPa. The brightness line profile clearly shows absorption by 2.5 μm Au foil between the Al_2O_3 buffer rod and the SiO_2 glass sample, and strong brightness contrast between the SiO_2 glass sample and Cu backing reflector. (b) Detected buffer rod/sample and sample/Cu interfaces from the image of Fig. 3(a).

distance in pixel from ambient condition. Uncertainty of the sample length determination was less than ± 1 pixel in a conservative estimation, because the buffer rod/sample and sample/backing reflector interface position was determined with the standard deviation of less than ± 0.2 pixel, respectively. The ± 1 pixel (0.948 μm) uncertainty in sample length determination corresponds to $\pm 0.26\%$ error in both compressional and shear wave velocity determination. We therefore consider that the overall uncertainty in the compressional and shear wave velocity measurement is less than $\pm 0.34\%$ and $\pm 0.30\%$, respectively.

III. STRUCTURE AND ELASTIC WAVE VELOCITIES OF SiO₂ GLASS UP TO 6.8 GPa AT ~500°C

Simultaneous structure and elastic wave velocity measurements were carried out for the SiO_2 glass sample up to 6.8 GPa at around 500°C. We first compressed the SiO_2 glass to 1.5 GPa at room temperature, and then heated to 500°C. Then we further compressed the sample at 500°C while collecting data at each pressure point. However, the thermocouple was broken at around 2–3 GPa, and then we kept a constant power, which generated 500°C at 1–2 GPa. We conducted ultrasonic and x-ray radiography measurements at all pressure steps and determined the pressure dependence of compressional (Vp) and shear (Vs) wave velocities. The structure of the SiO_2 glass was measured at 2.8, 4.5, 6.0, and 6.8 GPa. Since the structure measurement took around 2–3 h, we measured the ultrasonic and x-ray radiography before and after each structure measurement.

Figure 4 shows two-way travel times of compressional (2ΔTp) and shear (2ΔTs) waves. The arrows indicate the shift of two-way travel times during the structure measurements at 2.8, 4.5, 6.0, and 6.8 GPa. Both 2ΔTp and 2ΔTs significantly decreased during the structure measurement at 2.8 and 4.5 GPa, but the changes were marginal at 6 and
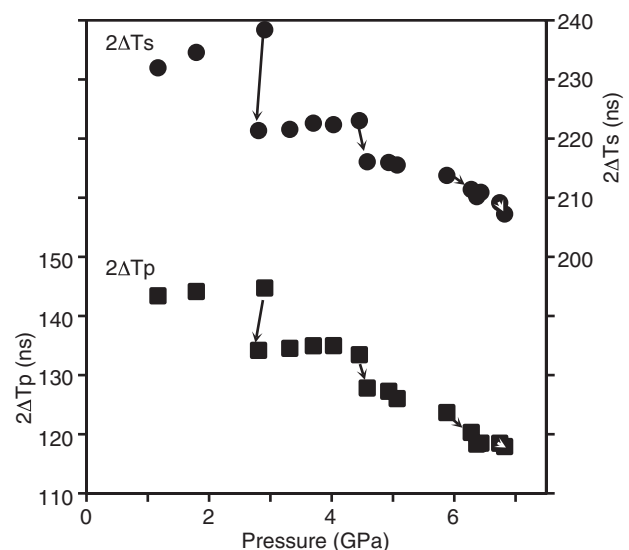
position caused by the Au foil absorption. In contrast, the position of the sample/backing reflector was defined at the middle position of the brightness between SiO_2 and Cu. The brightness of SiO_2 and Cu was derived by averaging the brightness of nearest 50 pixels, respectively. Figure 3(b) shows an example of the boundary analysis carried out for the image of Fig. 3(a). The boundary positions were determined by investigating the vertical profiles as function of horizontal pixel positions from 150 pixel to 1200 pixel with 1 pixel step. Sample/backing reflector interface was defined at almost all steps, while buffer rod/sample interface was not detected at some steps probably due to uncertainties in the automatic peak detection for variable peak shape and noise level. Then the obtained boundary position data were fitted to a linear equation to determine distance between buffer rod/sample and sample/backing reflector (= sample length). We first fit the buffer rod/sample boundary position data, and then we fit the sample/backing reflector interface data to the linear equation with the same slope as that of the buffer rod/sample boundary. Sample length at high pressure and high temperature conditions was calculated using a relative change of

FIG. 4. Variation of two-way travel times of compressional (2ΔTp) and shear (2ΔTs) waves with increasing pressure at around 500°C. The arrows indicate the 2ΔTp and 2ΔTs change during 2–3 h for multi-angle energy-dispersive x-ray diffraction measurement (see text for more descriptions).
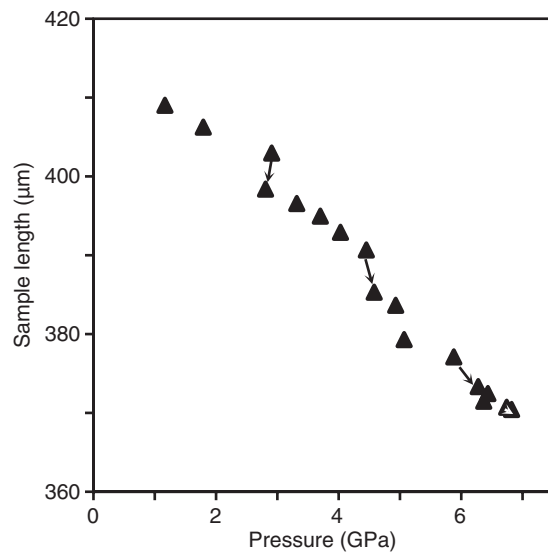
FIG. 5. Sample length change with increasing pressure. The arrows indicate sample length change before and after the multi-angle energy-dispersive x-ray diffraction measurement.

6.8 GPa. $2\Delta Tp$ and $2\Delta Ts$ increased with increasing pressure at the pressures of 1.2–2.9 GPa and 2.8–4.0 GPa, while started decreasing above 4.5 GPa. In contrast, sample length continuously decreased with increasing pressure (Fig. 5). Similarly to the two-way travel time change, sample length also changed during the structure measurement. But, the change of sample length (1.0%–1.5% at 2.8, 4.5, and 6 GPa) was noticeably smaller than the change of $2\Delta Tp$ and $2\Delta Ts$ (3%–8% change at 2.8 and 4.5 GPa). Some previous studies have demonstrated logarithmic time dependence in the volume change (e.g., Ref. 20) or Brillouin frequency shift (e.g., Ref. 21), which reflects elastic wave velocity change, at high pressure or high temperature conditions. Our observed $2\Delta Tp$, $2\Delta Ts$, and sample length change before and after the structure measurement in ∼2–3 h may be attributed to such time-dependent behavior of SiO_2 glass. However, pressure and temperature dependence of the time-dependent behavior of SiO_2 glass has not been well understood yet. We need further investigations particularly at simultaneous high pressure and high temperature conditions, in order to clarify pressure-temperature-time dependent kinetic behavior of SiO_2 glass.

Vp, Vs and Poisson's ratio ($=\frac{1}{2}[1 - \frac{1}{(Vp/Vs)^2 - 1}]$) were determined by using the observed two-way travel times and sample length (Fig. 6). We observed distinct up-shift of Vp and Vs during the structure measurement at 2.8 and 4.5 GPa, which reflects the down-shits of $2\Delta Tp$ and $2\Delta Ts$, respectively. Pressure dependence of Vp was negative at the pressures of 1.2–2.9 GPa and 2.8–4.0 GPa, but changed to positive above ∼5 GPa. Vs also decreased first with increasing pressure up to ∼4 GPa, while Vs was almost constant at around 4–6.8 GPa. In contrast, Poisson's ratio almost continuously increased with increasing pressure.

We compared the Vp, Vs, and Poisson's ratio observed at around 500°C with those at room temperature reported in Ref. 10. Vp, Vs, and Poisson's ratio at 1 GPa and 500°C was similar to those at room temperature, while Vp, Vs,
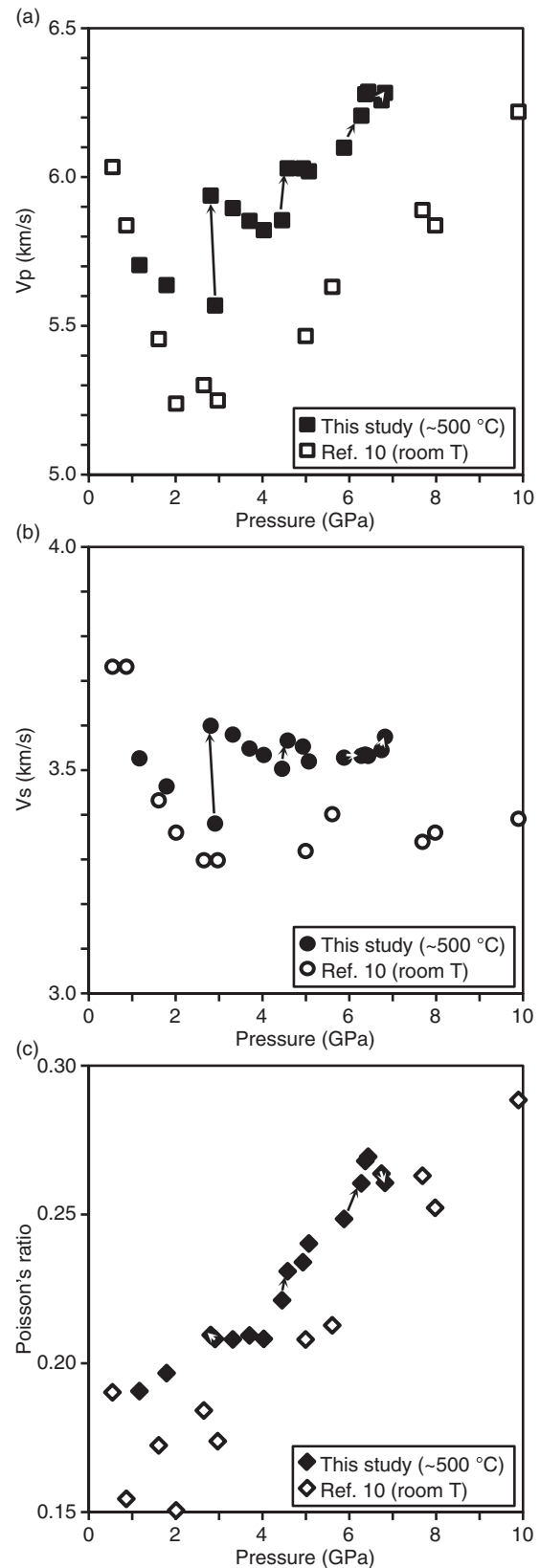

FIG. 6. (a) Compressional (Vp) and (b) shear (Vs) wave velocities, and (c) Poisson's ratio of SiO_2 glass as a function of pressure. Solid symbols represent Vp, Vs, and Poisson's ratio obtained in this study at ∼500°C, and open symbols are those at room temperature reported in Ref. 10. The arrows indicate Vp, Vs, and Poisson's ratio change during the multi-angle energy-dispersive x-ray diffraction measurement in this study.

and Poisson's ratio at 500°C become higher than those at room temperature above 2 GPa. Pressure dependence of Vp, Vs, and Poisson's ratio was similar between those at 500°C and room temperature, and Vp, Vs, and Poisson's ratio, respectively, showed around 0.6 km/s, 0.2 km/s, and 0.025 differences between ~500°C and room temperature. As the result, Vp observed at 6.8 GPa and ~500°C is same as that at around 10 GPa at room temperature. In contrast, because Vs showed almost no pressure dependence between around 4 and 10 GPa at room temperature (Ref. 10), Vs at 6.8 GPa and ~500°C was higher than that at ~10 GPa and room temperature. According to the results of Ref. 10, Vs at room temperature started increasing above 10 GPa, and the Vs value of 3.6 km/s at 6.8 GPa and ~500°C observed in this study was comparable to that at around 12 GPa at room temperature. In addition, Poisson's ratio showed similar trend as Vp, and the Poisson's ratio at 6.8 GPa and ~500°C was similar to that at around 8 GPa at room temperature.

Figure 7(a) shows structure factor S(Q) obtained by multi-angle energy-dispersive x-ray diffraction at 2.8, 4.5, 6.0, and 6.8 GPa. The arrows indicate position of the first sharp diffraction peak (FSDP) of the S(Q), which reflects the intermediate range ordering. It has been known that the position of FSDP substantially changes by densification (e.g., Refs. 22 and 23). In particular, Ref. 23 showed linear relation between the shift of FSDP position and density increase in SiO$_2$ glass. Our result showed that FSDP position shifted to higher Q with increasing pressure, in agreement with previous studies (e.g., Ref. 24) (Fig. 7). Our observed FSDP position at ~500°C is markedly higher than those at room temperature reported in Ref. 24 and is close to those observed at high temperatures. The somewhat smaller FSDP position value observed in this study above 4.5 GPa would be due to the difference of temperature condition between this study and Ref. 24, because the high temperature data of Ref. 24 are obtained at the highest temperature of ~650°C at 5.5 GPa, and they showed continuous shifting of the FSDP position to higher Q up to the highest temperature.

The FSDP position observed at 6.8 GPa and ~500°C roughly corresponds to that at around 9 GPa at room temperature if we interpolate the FSDP position of ~7.5 GPa and 10 GPa at room temperature reported in Ref. 24. The difference in the FSDP position between ~500°C and room temperature is similar to the difference of Vp and Poisson's ratio between ~500°C and room temperature (Fig. 6). Figure 8 shows comparison of the FSDP positions with Vp, Vs, and Poisson's ratio measured at the same pressure condition (2.8, 4.5, 6.0, and 6.8 GPa). Vp and Poisson's ratio proportionally increase with the shift of the FSDP position. In contrast, Vs does not show such correlation and is almost constant.

In order to obtain local structural information, we calculated the reduced pair distribution function G(r) by the Fourier transformation of S(Q) (Fig. 9(a)). We compared our observed Si-O and Si-Si distance of SiO$_2$ with those at room temperature reported in Ref. 17 (0 and 3 GPa) and Ref. 25 (0 and 8 GPa only for Si-O distance). Direct comparisons are difficult because previous studies mainly investigated the Si-O distance of SiO$_2$ glass above ~10 GPa (e.g.,
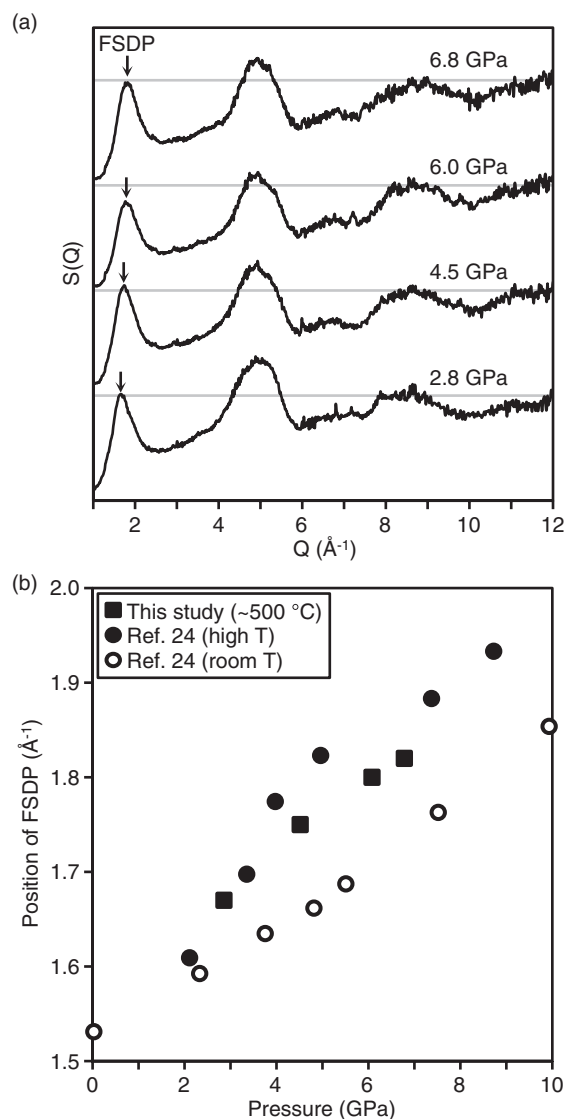

FIG. 7. (a) The structure factor S(Q) obtained at 2.8, 4.5, 6.0, and 6.8 GPa. The arrows indicate position of the first sharp diffraction peak (FSDP). (b) Pressure dependence of the position of FSDP. Solid symbols represent the results obtained at high temperature by this study and Ref. 24 and open symbols are the data obtained at room temperature reported in Ref. 24. The high temperature data of Ref. 24 are obtained at the temperature where the FSDP position shifting was finished.

Refs. 25 and 26). The Si-O distance at ~500°C is slightly larger than those obtained at room temperature (Fig. 9(b)). There is only marginal pressure dependence of the Si-O distance at ~500°C in the pressure range of this study, similar to the results obtained at room temperature (Ref. 25). In contrast, pressure dependence of Si-Si distance at ~500°C shows a turn-over between 4.5 and 6.0 GPa. The Si-Si distance increased between 2.8 and 4.5 GPa, but it decreased between 6.0 and 6.8 GPa. Since the Si-O distance is almost unchanged, the change in Si-Si distance would be attributed to the change of Si-O-Si angle. We estimated Si-O-Si angle using the relation between the distance of Si-O (r_{Si-O}) and Si-Si (r_{Si-Si}) (Si-O-Si angle $= 2\arcsin(r_{Si-Si}/2r_{Si-O})$). As a result, the Si-O-Si angle increased with increasing pressure up to 4.5–6.0 GPa and started decreasing at higher pressures (Fig. 9(b)). Molecular-dynamics study of Ref. 22 has
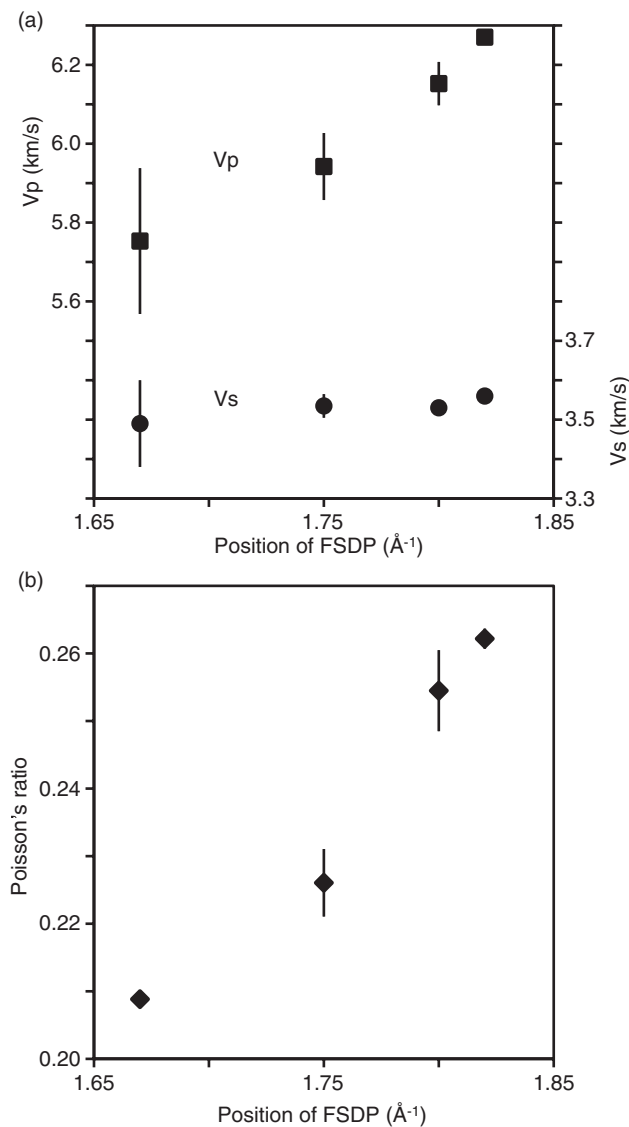
FIG. 8. Relationship between the position of FSDP and Vp, Vs (a), or Poisson's ratio (b). The Vp, Vs, and Poisson's ratio values are the average of those obtained before and after the structure measurement, and the vertical bars represent difference of Vp, Vs, or Poisson's ratio before and after the structure measurement.

FIG. 9. (a) The reduced pair distribution function G(r) calculated by the Fourier transformation of S(Q) (Fig. 7(a)). (b) Pressure dependence of the Si-O and Si-Si distance and the calculated Si-O-Si angle. Solid symbols represent the results obtained at high temperature and open symbols are the data obtained at room temperature.

suggested that densification of SiO_2 glass can be explained by the decrease of Si-O-Si angle and shortening of Si-Si distance. In addition, Ref. 24 showed that transition region between normal and highly densified glass started above ~3 GPa and finish at around 5.5–7.0 GPa at 500°C. These data are consistent with the start of decrease of Si-O-Si angle above 4.5–6.0 GPa obtained in this study, and therefore the turn-over of the Si-O-Si angle at 4.5–6.0 GPa and ~500°C might indicate the appearance of permanent densification in the SiO_2 glass.

Although a strong correlation was identified between the intermediate range ordering (FSDP position) and Vp or Poisson's ratio, there was no clear correlation between Si-O distance and Vp or Poisson's ratio, because Si-O distance was almost constant with varying pressure. In contrast, Vs was almost constant at 4.0–6.8 GPa, which might imply a possibility of connection of Vs behavior to this rigid Si-O distance.
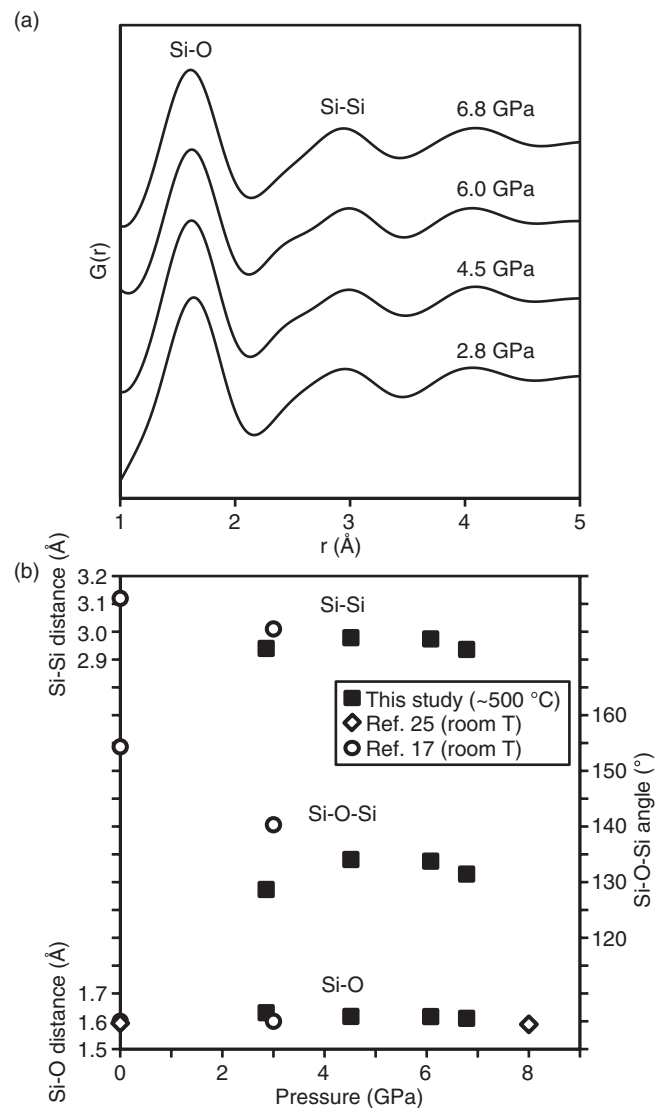
At room temperature, it has been reported that Vs stayed almost constant to around 12 GPa, and started increasing above 12 GPa (Ref. 10). The Si-O distance also started increasing above 8–15 GPa at room temperature (Refs. 25 and 26). Further studies are needed to address this issue.

Interestingly, a turn-over was observed in both Si-O-Si angle and pressure dependence of Vp at ~5 GPa (Figs. 6 and 9). Therefore, the turn-over of pressure dependence of Vp may be explained by the change in Si-O-Si angle. The turn-over of pressure dependence of Vp and Vs has been observed at room temperature (e.g., Refs. 10 and 14). Vp and Vs of SiO_2 glass first decrease with increasing pressure up to around 2–4 GPa, then start increasing at higher pressures. This behavior is the same as those observed at ~500°C, although the turn-over pressure is somewhat higher for the high temperature sample. In contrast, behavior of Si-O-Si angle looks different between ~500°C and room temperature. Reference 17 showed a decrease of Si-O-Si angle between 0

and 3 GPa at room temperature, but our data show an increase of Si-O-Si angle at 2.8–4.5 GPa at around 500°C. Because the local structure data such as Si-O distance and/or Si-O-Si angle is limited, it is difficult to reconcile this discrepancy. Further structural studies are required to clarify this particular observation.

IV. CONCLUSION

A new setup of combined multi-angle energy-dispersive x-ray diffraction with ultrasonic and x-ray radiography measurement allows us to simultaneously investigate structure and elastic wave velocities of amorphous materials at high pressure and high temperature conditions, thus the *in situ* correlations. The first simultaneous structure and elastic wave velocity measurement on SiO$_2$ glass revealed a strong correlation between FSDP position and Vp or Poisson's ratio. Vp and Poisson's ratio proportionally increases with the shift of FSDP position. In contrast, Si-O distance was almost constant at the pressure range in this study. These data imply that the change of Vp and Poisson's ratio under current pressure range is mainly influenced by intermediate range ordering rather than short range order structures. In contrast, Vs was almost constant above 4 GPa, and there was no correlation between Vs and FSDP position. Vs might be more sensitive to local structure than the intermediate range structure. Further study of simultaneous structure and elastic wave velocity measurements using the new setup should provide better constraints on the correlation between structure and elastic wave velocities of SiO$_2$ glass.

The setup opens a new way to investigate the link between microscopic structure and macroscopic elastic wave velocities of amorphous materials at high pressure and high temperature conditions. Although the current experiment was carried out only for glass, the new setup should also be applicable for the study of liquids or melts. Actually, structures of liquids/melts have been investigated in the PE cell (e.g., Ref. 4). Although elastic wave velocity measurement of liquids/melts at high pressure and high temperature conditions is still challenging, some recent studies have reported pioneering ultrasonic measurement of liquid mercury (Ref. 27) up to 5 GPa and 303°C and liquid sodium (Ref. 28) up to 2 GPa and 220°C. Further modification of our cell assembly to enclose liquid sample in the PE cell should enable us to investigate both structure and elastic wave velocities of liquids simultaneously at high pressure and temperature conditions.

Another recent PE cell experiment of the combined ultrasonic and microtomography measurements at the Sector 13-BM-D, GSECARS at the APS has demonstrated a capability to determine elastic wave velocity and density of amorphous materials simultaneously (Ref. 11). Combination of these techniques with the current new setup of simultaneous ultrasonic and multi-angle energy dispersive x-ray measurements should provide more implication for a comprehensive understanding of structure, elasticity, and equation of state of amorphous materials at high pressure and high temperature conditions.

[1] K. Tsuji, K. Yaoita, M. Imai, O. Shimomura, and T. Kikegawa, Rev. Sci. Instrum. **60**(7), 2425–2428 (1989).
[2] M. Mezouar, P. Faure, W. Crichton, N. Rambert, B. Sitaud, S. Bauchau, and G. Blattmann, Rev. Sci. Instrum. **73**(10), 3570–3574 (2002).
[3] G. Shen, V. B. Prakapenka, M. L. Rivers, and S. R. Sutton, Rev. Sci. Instrum. **74**(6), 3021–3026 (2003).
[4] A. Yamada, Y. Wang, T. Inoue, W. Yang, C. Park, T. Yu, and G. Shen, Rev. Sci. Instrum. **82**(1), 015103–015107 (2011).
[5] Y. Katayama, K. Tsuji, O. Shimomura, T. Kikegawa, M. Mezouar, D. Martinez-Garcia, J. M. Besson, D. Hausermann, and M. Hanfland, J. Synchrotron Radiat. **5**(3), 1023–1025 (1998).
[6] G. Shen, N. Sata, M. Newville, M. L. Rivers, and S. R. Sutton, Appl. Phys. Lett. **81**(8), 1411–1413 (2002).
[7] E. Ohtani, A. Suzuki, R. Ando, S. Urakawa, K. Funakoshi, and Y. Katayama, in *Advances in High-Pressure Technology for Geophysical Applications*, edited by J. Chen, Y. Wang, T. S. Duffy, G. Shen, and L. F. Dobrzhinetskaya (Elsevier, Amsterdam, 2005), pp. 195–210.
[8] C. E. Lesher, Y. Wang, S. Gaudio, A. Clark, N. Nishiyama, and M. Rivers, Phys. Earth Planet. Interiors **174**(1–4), 292–301 (2009).
[9] J.-P. Perrillat, M. Mezouar, G. Garbarino, and S. Bauchau, High Press. Res. **30**(3), 415–423 (2010).
[10] C.-S. Zha, R. J. Hemley, H.-K. Mao, T. S. Duffy, and C. Meade, Phys. Rev. B **50**(18), 13105–13112 (1994).
[11] Y. Kono, A. Yamada, Y. Wang, T. Yu, and T. Inoue, Rev. Sci. Instrum. **82**(2), 023906–023907 (2011).
[12] Y. Greenberg, E. Yahel, R. Ganor, R. Hevroni, I. Korover, M. P. Dariel, and G. Makov, J. Non-Cryst. Solids **354**(34), 4094–4100 (2008).
[13] M. Murakami and J. D. Bass, Phys. Rev. Lett. **104**(2), 025504 (2010).
[14] A. Yokoyama, M. Matsui, Y. Higo, Y. Kono, T. Irifune, and K.-i. Funakoshi, J. Appl. Phys. **107**(12), 123530–123535 (2010).
[15] J. M. Besson, R. J. Nelmes, G. Hamel, J. S. Loveday, G. Weill, and S. Hull, Physica B **180–181**, 907–910 (1992).
[16] L. S. Dubrovinsky, S. K. Saxena, and P. Lazor, Phys. Chem. Miner. **25**(6), 434–441 (1998).
[17] K. Funakoshi, Ph.D. dissertation, Tokyo Institute of Technology, 1997.
[18] D. Lheureux, F. Decremps, M. Fischer, A. Polian, J. P. Itié, G. Syfosse, and A. Zarembowitch, Ultrasonics **38**(1–8), 247–251 (2000).
[19] Y. D. Sinelnikov, G. Chen, and R. C. Liebermann, High Press. Res. **24**(1), 183–191 (2004).
[20] O. B. Tsiok, V. V. Brazhkin, A. G. Lyapin, and L. G. Khvostantsev, Phys. Rev. Lett. **80**(5), 999–1002 (1998).
[21] V. G. Karpov and M. Grimsditch, Phys. Rev. B **48**(10), 6941–6948 (1993).
[22] S. Susman, K. J. Volin, D. L. Price, M. Grimsditch, J. P. Rino, R. K. Kalia, P. Vashishta, G. Gwanmesia, Y. Wang, and R. C. Liebermann, Phys. Rev. B **43**(1), 1194–1197 (1991).
[23] Y. Inamura, M. Arai, N. Kitamura, S. M. Bennington, and A. C. Hannon, Physica B **241–243**, 903–905 (1997).
[24] Y. Inamura, Y. Katayama, W. Utsumi, and K.-i. Funakoshi, Phys. Rev. Lett. **93**(1), 015501 (2004).
[25] C. Meade, R. J. Hemley, and H. K. Mao, Phys. Rev. Lett. **69**(9), 1387–1390 (1992).
[26] C. J. Benmore, E. Soignard, S. A. Amin, M. Guthrie, S. D. Shastri, P. L. Lee, and J. L. Yarger, Phys. Rev. B **81**(5), 054105 (2010).
[27] F. Decremps, L. Belliard, B. Couzinet, S. Vincent, P. Munsch, G. Le Marchand, and B. Perrin, Rev. Sci. Instrum. **80**(7), 073902–073903 (2009).
[28] W. Song, Y. Liu, Z. Wang, C. Gong, J. Guo, W. Zhou, and H. Xie, Rev. Sci. Instrum. **82**(8), 086108–086103 (2011).